Four terminal-pair measurements of ceramic capacitors

S. Schlamminger, J. Love, A. Koffman, Y. Wang
National Institute of Standards and Technology
Gaithersburg, Maryland 20899

***Abstract*—Expanding on our previous work on four terminal-pair air capacitors, we present a model for the frequency-dependent capacitance of ceramic capacitors for values ranging from 10 nF to 10 µF. Two measurements are necessary to completely model the frequency dependence of the capacitance. First, the location of the pole in the admittance in the frequency range from 100 kHz to 20 MHz. This measurement is obtained with a vector network analyzer. Second, the dissipation factor at 1 kHz can be measured with a capacitance bridge. From these two measurements, the relative change in frequency for frequencies ranging from 100 Hz to 100 kHz can be constructed.**

I. Obtaining admittance with a VNA

A recent article [1] demonstrates the use of a four-channel vector network analyzer (VNA) to measure the four terminal-pair impedance of air capacitors. The present abstract extends this work to ceramic capacitors. The measurement problem is to establish the relative change of capacitance, ε as a function of frequency with respect to the value $C(f_0)$ measured at a low frequency, typically $f_0 = 1\,\mathrm{kHz}$. We define

$$\varepsilon := \frac{C(f)}{C(f_0)} - 1. \tag{1}$$

According to textbooks for microwave engineering, e.g. [2], the impedance matrix, $\mathbf{Z}$, can be obtained from the 16 components of the S-parameter matrix $\mathbf{S}$ and the identity matrix $\mathbf{I}$, using

$$\mathbf{Z} = Z_t \cdot (\mathbf{I} + \mathbf{S}) \times (\mathbf{I} - \mathbf{S})^{-1}, \tag{2}$$

where Z_t is the load impedance, which is $50\,\Omega$ for most VNAs. The components of the matrix $\mathbf{Z}$ are denoted as z_{ij} with $i, j \in \{1, 2, 3, 4\}$ and are frequency dependent. Only four of the 16 components of $\mathbf{Z}$ are required to calculate the four terminal-pair capacitance via

$$Z_{4\mathrm{TP}} = -z_{24} + \frac{z_{21} z_{34}}{z_{31}}. \tag{3}$$

For the rest of the article, we will work in the admittance domain, and we will leave out the 4TP subscript. The admittance is

$$Y = \frac{1}{Z_{4\mathrm{TP}}}. \tag{4}$$

The frequency-dependent capacitance C and dissipation factor D are obtained as

$$C = \frac{\mathrm{Im}(Y)}{2\pi f}, \quad D = \frac{\mathrm{Re}(Y)}{\mathrm{Im}(Y)}, \tag{5}$$

respectively.

Fig. 1 shows the complete data obtained for the four capacitors under test with nominal values of 10 nF, 100 nF, 1 µF, and 10 µF.

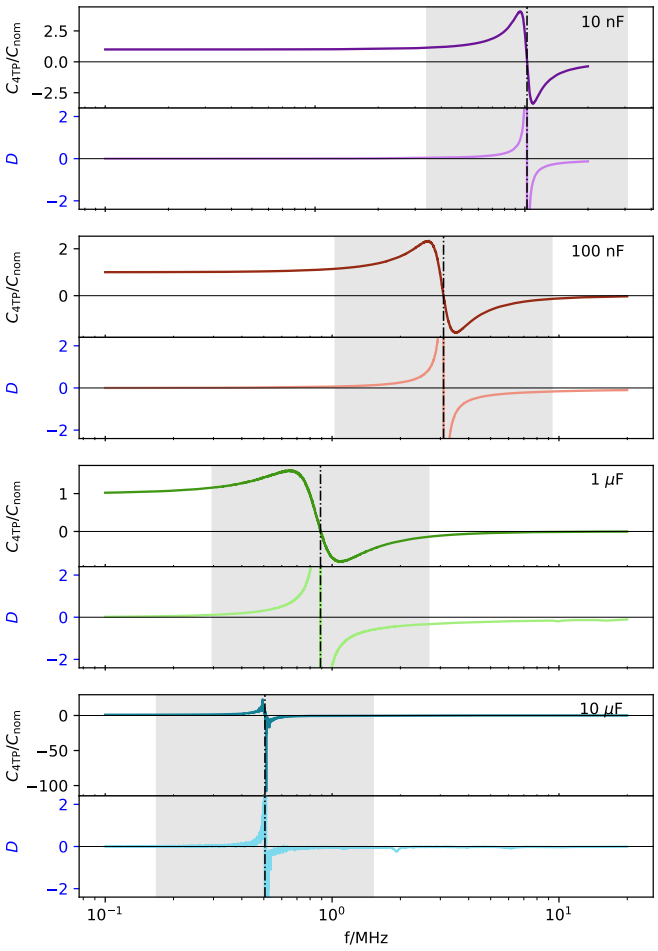

Fig. 1. The complete data set obtained with the VNA shown as C and D for frequencies ranging from 100 kHz to 20 MHz. The dash-dotted line marks the position of the pole, f_p. The grey shaded area is the fitting region used below, defined as $f_p/3 \le f \le 3f_p$.

II. Measured low-frequency behaviour

By inspecting the data, it is found for frequencies above 100 kHz, the capacitance scales proportionally to f^2 with a

TABLE I

RESULTS FOR THE PARAMETER $a_{\rm fit}$ FITTING EQ. (6) AND a_{pole} ACCORDING TO EQ. (16). THE LAST COLUMN SHOWS THE DIFFERENCE, $a_{pole} - a_{fit}$. THE NUMBER IN PARENTHESES GIVES THE 1-σ UNCERTAINTIES OF THE APPROPRIATE DIGITS.

$C_{\rm nom}$	$a_{\rm fit}$ /MHz^{-2}	$a_{\rm pole}$ /MHz^{-2}	$\frac{(a_{\rm fit}-a_{\rm pole})}{a_{\rm fit}}$
10 nF	$1.057(3) \times 10^{-2}$	$9.4(2) \times 10^{-3}$	0.11(2)
100 nF	$1.335(7) \times 10^{-1}$	$9.6(2) \times 10^{-2}$	0.28(2)
1 µF	1.7(1)	0.93(3)	0.46(6)
10 µF	4(1)	3.891	0.0(3)

small f^4 admixture, consistent with a simple LC resonance model i.e.,

$$C(f) = C(f_0)\left(1 + a_{\rm fit} f^2 + b_{\rm fit} f^4\right). \quad (6)$$

Fits of this function to the measured data are shown in Fig. 2 for all four capacitors. The fitted lines and the residuals are also shown in the figure. The results of the dominant fit parameter $a_{\rm fit}$ are listed with 1-σ uncertainties in Tab. I.

In [1], it was shown that the coefficients a and b can be obtained from the location of the poles and zeros, respectively. For the capacitors investigated here, only one pole and no zeros exist in the measurement range from 100 kHz to 20 MHz as can easily be verified by looking at Fig. 1.

In this case, the a coefficient is given by

$$a_{\rm pole} = \frac{1}{f_p^2}, \quad (7)$$

where f_p is the location of the pole. Note, the subscripts $_{\rm pole}$ and $_{\rm fit}$ are used to distinguish how the numerical value of a is obtained.

The single pole per capacitor in the frequency range from 100 kHz and 20 MHz can easily be found in Fig. 1. However, The poles are not as sharp as those found for the air capacitors in [1]. In the next section, we investigate the effect of damping on $a_{\rm pole}$.

III. INTERPRETING THE ADMITTANCE

While the methodology of obtaining Y from the VNA measurements is identical for air and ceramic capacitors, there is a difference in interpreting the measurements and in obtaining the frequency dependence of C. That difference stems from the fact that the poles of the air capacitor are close to the imaginary axis in the Laplace plane, i.e., their real component is negligible. This assumption is not correct for the more lossy ceramic capacitors, as is discussed below.

The simplest lumped circuit model of a lossy capacitor is shown in Fig. 3. The circuit includes inductance and resistance in series with an ideal capacitor. The differential equation for the voltage u and a function of current i is

$$u = R_s i + L_s \frac{{\rm d}i}{{\rm d}t} + \frac{1}{C_0}\int i {\rm d}t \quad (8)$$

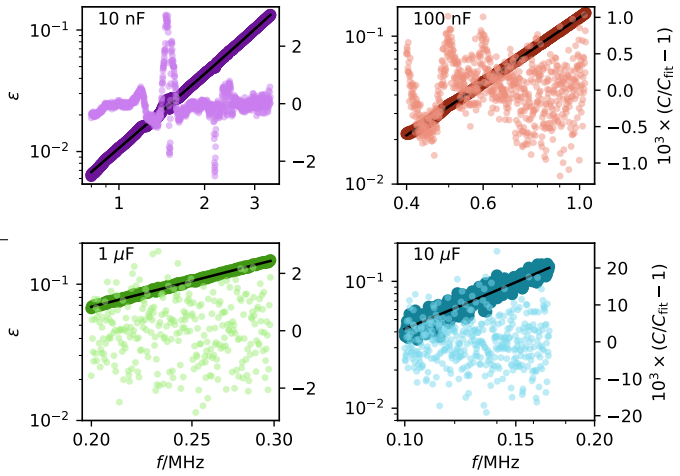

Fig. 2. The measured four terminal-pair capacitances as a function of frequency are shown as the dark-colored points with the scale on the left. Fits by the equation $\varepsilon = a_{\rm fit} f^2 + b_{\rm fit} f^4$ are shown as black lines. The fit residuals are plotted in lighter colors and are referenced to the right vertical scale.

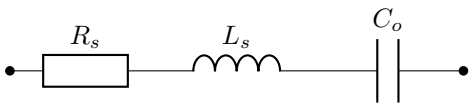

Fig. 3. Lumped circuit model including the resistivity and inductivity of the leads.

We utilize the Laplace transformation, a tool commonly used in control theory, to obtain the transfer function in the frequency domain. It is

$$Y(s) = \frac{I(s)}{U(s)} = \frac{C_0 s}{L_s C_0 s^2 + R_s C_0 s + 1}.. \quad (9)$$

The capital letters $U(s)$ and $I(s)$ indicate here that voltage and current are given in the Laplace domain. The transfer function in the frequency domain can be obtained by assigning $s = j\,2\pi f$, where j is the imaginary unit. With the abbreviations,

$$\omega_o = 2\pi f_o = \sqrt{\frac{1}{L_s C_o}}, \quad \tau = R_s C_o, \quad \text{and} \quad \omega = 2\pi f, \quad (10)$$

Eq. (9) can rewritten as

$$Y(s) = C_0\omega_0^2 \frac{s}{s^2 + \tau\omega_0^2 s + \omega_0^2} = C_0\omega_0^2 \frac{s}{(s-p)(s-\bar{p})}, \quad (11)$$

where the second equation clearly indicates that the transfer function has one zero at $s = 0$ and a pair of complex conjugate poles at $s = p$ and $s = \bar{p}$. One pole is at

$$p = -\frac{1}{2}\tau\omega_0^2 + j\,\omega_0\sqrt{1 - \frac{1}{4}\tau^2\omega_0^2} \quad (12)$$

and the other at its complex conjugate.

We fit $Y(j2\pi f)$, given by Eq. 11 to the measured data. Only data within a frequency range of $f_0/3 \le f \le 3f_0$ were used for this fit. The data and the fitted function are shown

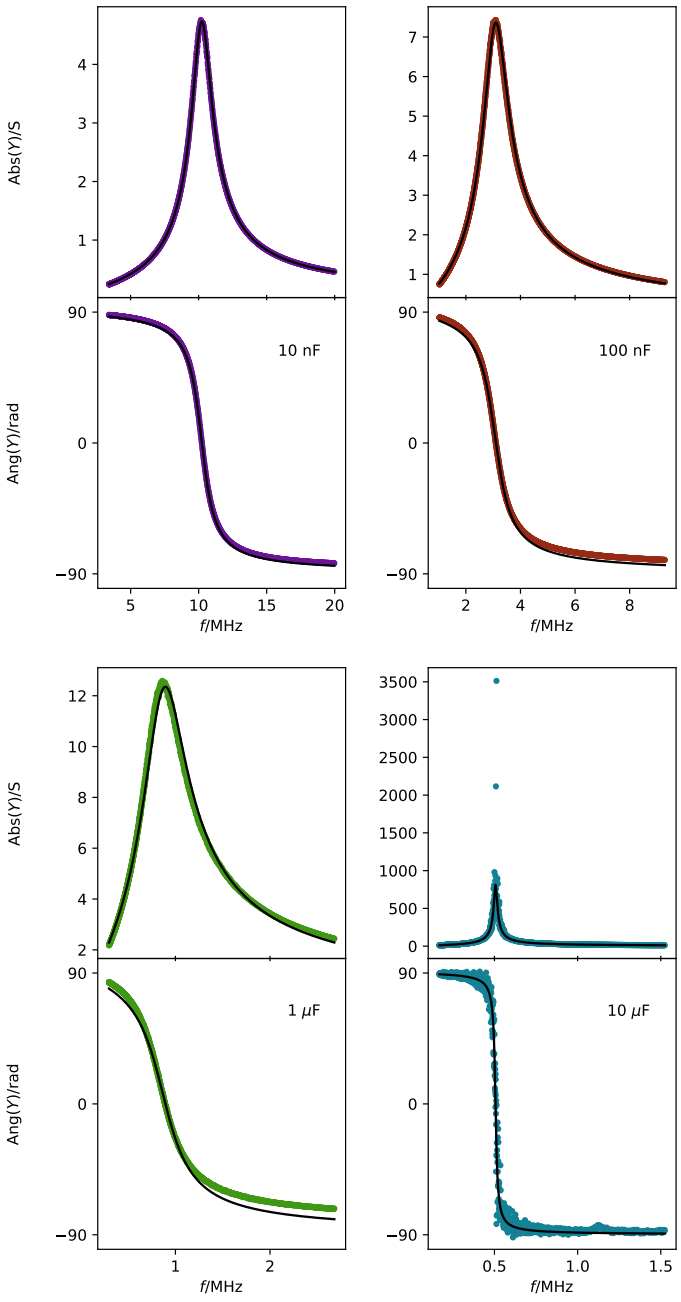

Fig. 4. Measured data $|Y|$ and $\angle Y$ for $Y(j2\pi f)$ as a function of f shown as colored points. The black lines are fit to Eq. 11.

in Fig. 4. The parameters τ and $\omega_0 = 2\pi f_0$ can be obtained from the fit; see Tab. II. The fit will also return an estimate for C_0, but it has a large uncertainty and is discarded. The right two columns of the table give the values for R_s and L_s that can be calculated from the fit results using Eq. 10.

From the fit, the pole location in the complex plane can be obtained; see Figure 5. The plots on the right show the real and imaginary parts of p as a function of the nominal capacitance. The dot-dashed lines represent fits to the lower three data points with a given slope. The real part is proportional to

TABLE II

POLE FIT RESULT. COLUMNS TWO AND THREE GIVE THE RESULTS OF THE FIT PARAMETERS FOR THE BEST FIT. THE COLUMNS LABELED R_s AND L_s ARE CALCULATED FROM THESE PARAMETERS.. THE DIGITS' 1-σ UNCERTAINTIES ARE INDICATED IN PARENTHESES ALONGSIDE THEIR RESPECTIVE NUMBERS. FOR THE ENTRIES WITH MISSING UNCERTAINTIES, THEY ARE SMALLER THAN THE GIVEN PRECISION.

C_{nom}	f_0 /MHz	τ /ns	R_s /mΩ	L_s /nH
10 nF	10.23(4)	2.2(3)	217(53)	24.2(4)
100 nF	3.10(1)	14.4(6)	143(13)	26.4(4)
1 μF	0.894(2)	89.4(17)	89(3)	31.7(3)
10 μF	0.506	12.02(1)	1.19	9.8

$C_0^{-1/4}$. The theory, however, yields,

$$-\mathrm{Re}(p) = \frac{1}{2}\tau\omega_0^2 = \frac{1}{2}\frac{R_s}{L_s}. \tag{13}$$

Since, according to Table II, L_S is nearly constant for the three smaller valued capacitors, it requires $R_s \propto C_0^{-1/4}$. For the lower three capacitance values, the imaginary part shows a dependence of $C_0^{-1/2}$, which one would expect for $\omega_0\tau \ll 1$. In this case,

$$\mathrm{Im}(p) \approx \omega_0 = (L_s C_0)^{-1/2}, \tag{14}$$

which is proportional to $C_0^{-1/2}$ if L_s is constant. Hence, for the lower three capacitance values, the pole location is a parabola since $-\mathrm{Re}(p) \propto C_0^{-1/4}$ and $\mathrm{Im}(p) \propto C_0^{-1/2}$. The left plot shows the upper left quadrant of the complex plane and the poles with positive imaginary parts for the four capacitors. The black dot-dashed line corresponds to the appropriate combination of the two dashed-doted lines in the right plots. The combination explains the quadratic behavior seen by the points.

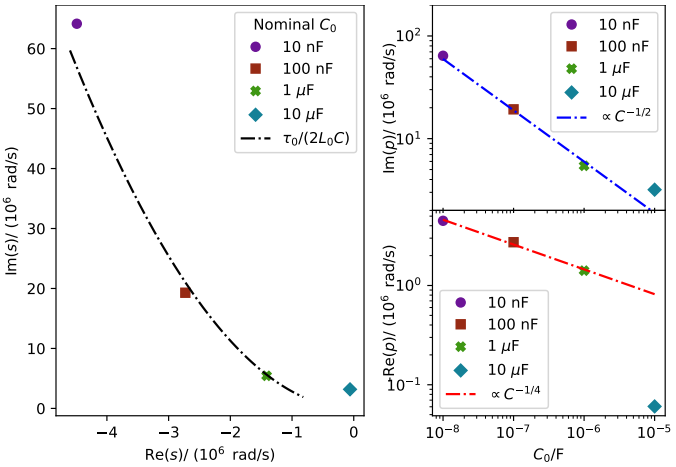

Fig. 5. Left panel shows the location of the poles in the second quadrant of the s-plane. The plots on the right show the negative real and positive imaginary part of the pole as a function of capacitance.

In all three graphs of Fig. 5, the pole location of the 10 μF capacitor is an outlier. Its construction must be different. This

fact can also be observed in Table II. The serial inductance for this capacitor is about three times smaller than the other capacitors.

IV. The frequency dependence of C above 100 kHz

The purpose of fitting the pole near the resonance frequency f_0 is to obtain information for $C(f)$ for $100\,\mathrm{kHz} < f \ll f_0$. Performing a Taylor expansion up to the second order in f of the combination of Eq. (5) and Eq. (9) yields

$$C = C_0 \left(1 + f^2 \left(\frac{1}{f_o^2} - 4\pi^2\tau^2\right)\right) \tag{15}$$

For $\omega \ll \omega_o$, $C = \mathrm{Im}(Y)/\omega^2$ can be developed in a Taylor series, and we obtain for ε,

$$\varepsilon = f^2 a_{\mathrm{pole}} \text{ with } a_{\mathrm{pole}} := \left(\frac{1}{f_o^2} - 4\pi^2\tau^2\right) \tag{16}$$

The value obtained for a_{pole} with the equation above can be compared to the a_{fit} which are obtained from polynomial fits to C for frequencies above 100 kHz to $1/3 f_p$. A detailed comparison with uncertainty is shown in Tab. I. Except for the 1 µF capacitor, the agreement is acceptable, with relative differences below 30 %.

V. Low frequency behaviour

The sections above describe the behavior of the capacitors above 100 kHz to below the first pole, which is given mainly by the coefficient a. For air capacitors, the low-frequency behavior is determined by the same coefficient, and the frequency-dependent part of the capacitance can be extrapolated down to audio frequencies. This extrapolation does not work for ceramic capacitors, due to the frequency dependence of the dielectric constant of the ceramic material.

A method to quantify the frequency dependence of the capacitance at audio frequencies is given in [3]. This method utilizes the Kramers-Kronig relationship to connect the change in capacitance to the dissipation factor. The authors of [3] found for audio frequencies,

$$\frac{C(f)}{C(f_0)} - 1 \approx -\frac{2}{\pi} D(f_0) \ln\left(\frac{f}{f_o}\right), \tag{17}$$

where D is the dissipation factor, defined by Eq. 5. Note, the approximate sign is necessary because we are using here $D(f_0)$ instead of $\tan(D(f))$ as is the case in the original paper. This approximation is justified since $D(f_0) \ll 1$ and is nearly frequency independent for low frequency D. At audio frequencies, $C(f)$ and $D(f)$ can be measured with a conventional capacitance bridge.

For $f_0 = 1$ kHz the dissipation factors for all four capacitors are a few parts in 1×10^5 with values of $3.2(15) \times 10^{-5}$, $2.6(20) \times 10^{-5}$, $4.2(50) \times 10^{-5}$, and $-0.2(25) \times 10^{-4}$ for the 10 nF, 100 nF, 1 µF, and 10 µF, respectively. Combining Eq. 17 with 6, yields

$$\varepsilon \approx -\frac{2}{\pi} D(f_0) \ln\left(\frac{f}{f_o}\right) + af^2 + bf^4. \tag{18}$$

We used a capacitance bridge to measure $C(f)$ for $f \in \{100\,\mathrm{Hz}, 1\,\mathrm{kHz}, 10\,\mathrm{kHz}, 100\,\mathrm{kHz}\}$. The measurements are shown in Fig. 6. Also shown in the figure are the calculated values for ε from Eq. (18). The agreement between the measured values and the model is good. The effect of the low-frequency correction, eq. 17 is most visible for the 10 nF capacitor because its a is lowest due to the high frequency of the pole, see Eq. (16). Hence, the entire extent of the plot is only 4×10^{-5}.

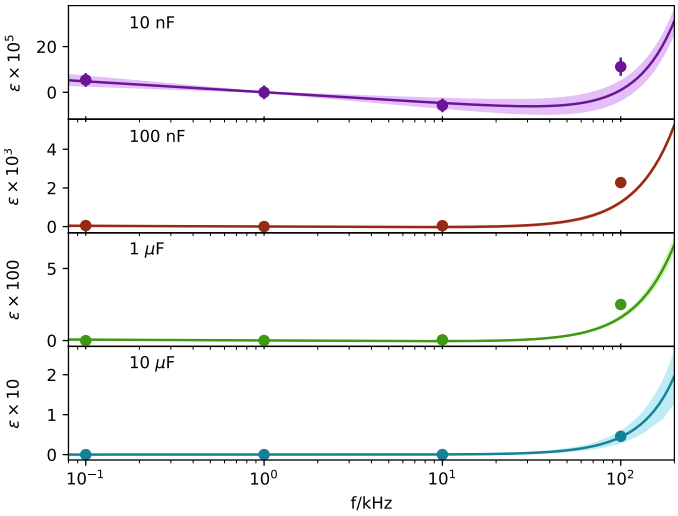

Fig. 6. Normalized measurements of the capacitors for four discrete frequencies ranging from 100 Hz to 100 kHz. These measurements were performed with a capacitance bridge. The lines show the calculated value for ε according to Eq. 18. The shaded area indicates the 1σ standard uncertainty band of the calculation. Throughout this article, only Type A uncertainties are considered.

VI. Conclusion

We present a model for the frequency dependency of four terminal pair ceramic capacitors ranging in values for 10 nF to 10 µF. The model can predict the relative change in the capacitance from 100 Hz to 100 kHz. Two parameters are needed to calculate the model. First, The dissipation factor of the capacitor at 1 kHz can be obtained with a capacitance bridge. Second, the location of the pole of Y can be measured with a vector network analyzer. For the capacitors investigated here, the pole location is well below 20 MHz. The model describes the relative change of the capacitance with sufficient accuracy to be useful for secondary calibration.

References

[1] S. Schlamminger *et al*, Measurement of the frequency dependence of four terminal-pair air capacitors with a vector network analyzer, *IEEE Trans. Instrum. Meas.* **72** 8006410, 2023.

[2] D.M. Pozar, Microwave Engineering, 4th Ed. J. Wiley & Sons, 2012.

[3] Y. Wang, A.D. Koffman, G.J. Fitzpatrick, Dissipation factors of fused-silica capacitors in the audio frequency range, *IEEE Trans. Instrum. Meas.* **56** 624, 2007.